J. Fluid Mech. (1973), *vol.* 59, *part* 1, *pp.* 1–21
Printed in Great Britain

Experiments on nonlinear interactions in the transition of a free shear layer

By RICHARD W. MIKSAD

Department of Mathematics, Imperial College, London†

(Received 3 July 1972)

An experimental study is made of nonlinear interactions in a laminar free shear layer. Two disturbances (f_1 and f_2), excited by sound, amplify and grow independently for small amplitudes. At larger amplitudes the disturbances interact to generate fluctuations of sum and difference frequencies ($f_2 \pm f_1$). Harmonics and subharmonics of f_1 and f_2 are also generated and all fluctuations interact to generate additional fluctuations of the form $(nf_2/m) \pm (pf_1/q)$; $n, p = 1, 2, 3, \ldots$, $m, q = 1, 2$. Nonlinear mode competition suppresses the growth of f_1 or f_2, depending on their relative amplitudes, and contributes to finite amplitude equilibration. An upper bound on the modal integral of total $u'^2_{\text{r.m.s.}}$ fluctuation energy is found. Fluctuation energy tends to be distributed among all possible frequency components, and its upper bound does not increase as the number of components increases.

1. Introduction

An important feature of any naturally occurring flow is the presence of many disturbances which can cause instability and which can subsequently interact with one another when they grow to sufficiently large amplitudes. Sato (1970) observed the generation of sum and difference fluctuations in the instability of a laminar wake. These frequency components arise from the interaction of disturbances and must play an important role in turbulence, where many fluctuations are present.

In an attempt to model this feature of natural flows, the present experiments, like those of Sato (1970), were designed such that two unstable modes, f_1 and f_2, of the free shear layer could be simultaneously excited. f_2 is the most unstable mode of the shear layer and f_1 is a less unstable, lower frequency fundamental mode. f_1 was chosen to be the fundamental frequency which local stability calculations predicted to be the most unstable mode of the measured mean velocity field at the point where nonlinear interactions start to become important.

In Sato's experiments, two unstable modes of a symmetric laminar wake were excited. Their frequencies differed by 10%. The present experiments consider the problem of exciting two unstable modes of a laminar asymmetric free shear

† Present address: Division of Atmospheric Science, University of Miami, Miami, Florida.

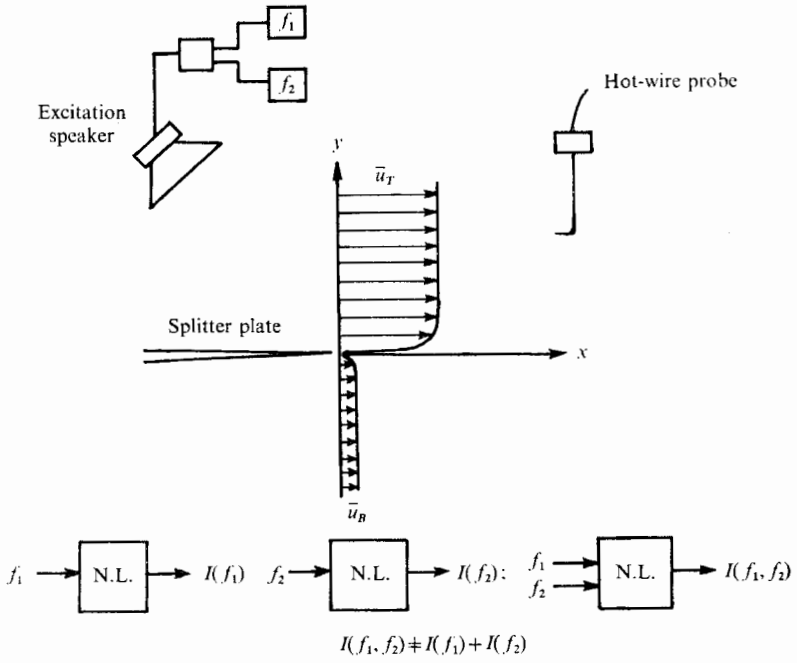

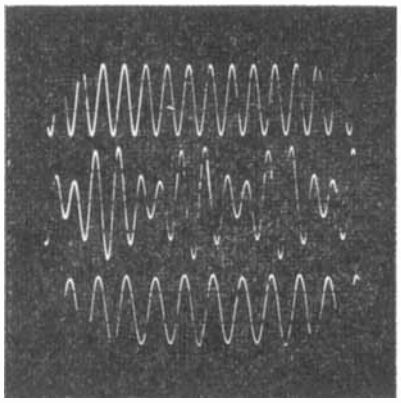

(*b*)

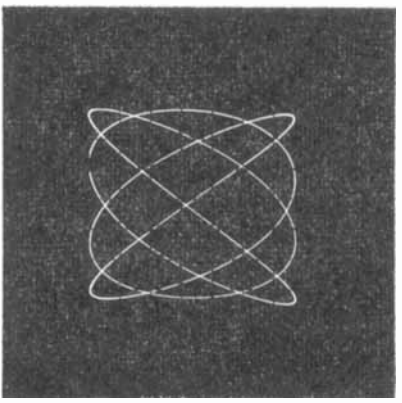

(*c*)

FIGURE 1. (*a*) Schematic of experimental set-up and initial mean velocity field. The three instabilities studied are indicated below, where the shear layer is pictured as a nonlinear black box. $I(f_1)$ is instability excited at f_1. $I(f_2)$ is instability excited at f_2. $I(f_1, f_2)$ is instability excited at f_1 and f_2 simultaneously. (*b*) Excitation signal for: $f_2 = 22{\cdot}5$ Hz instability (bottom); $f_1 = 29{\cdot}5$ Hz instability (top); $f_1 = 22$ Hz, $f_2 = 29{\cdot}5$ Hz dual instability (middle). (*c*) Lissajous phase pattern for f_1 and f_2 in the dual-excitation instability.

layer whose frequencies differ by 25%. Although the experiment differs from Sato's in mean flow and excitation frequencies, basic similarities are observed. The experiments are an extension of those of Miksad (1972), which studied the natural and excited instability of a free shear layer.

2. Experimental procedure

The basic apparatus was the low turbulence, open-return wind tunnel described in Miksad (1972). Disturbance fluctuations were excited by sound, and measurements made with a Shapiro–Edwards Model 50 constant-current hot-wire anemometer. Two excitation signals, obtained from a common reference signal, were fed to an audio amplifier and then to a loudspeaker. The ratio of the excitation frequencies was $f_1 : f_2 \simeq 3:4$. The relative phase of the signals was constant during the experiments. Sound disturbances were injected into the upper stream only. The injected disturbance field was of order 10^{-3} r.m.s. measured in terms of $\bar{u}_T$, the velocity of the upper stream. The respective excitation amplitudes of f_1 and f_2 could be varied, but were normally set equal. The excited instabilities grew with downstream distance and were initially described by spatial linear instability theory.

In order to determine which of the subsequent nonlinear features of instability were due to cross-interactions between the two excited fundamentals, the experiments were run in three stages, and in effect the shear layer was treated as a classic nonlinear black box. As indicated in figure 1, the features of instability due to cross-interactions between f_1 and f_2 were identified by comparing the dual-excitation instability with instabilities excited at f_1 or f_2 alone. These latter two experiments served to identify the nonlinear effects which occur when cross-interactions are not possible, and only self-induced nonlinear mechanisms are present. As noted in figure 1, the dual-excitation instability was not in general a simple superposition of the two instabilities excited at f_1 and f_2 individually. Superposition only held in those regions of instability where the disturbance amplitudes were very small.

3. Mean velocity field

Figure 2(*a*) shows the mean velocity field $\bar{u}(x, y)$ when $f_1 = 22$ Hz and $f_2 = 29{\cdot}5$ Hz are simultaneously excited. x is the downstream distance and y is normal to x and to the mean vorticity vector. The mean velocity fields during natural instability and during excitation at $f_2 = 29{\cdot}5$ Hz are given in Miksad (1972). Note the close similarity of the velocity field in the present experiments to that measured by Miksad during excitation at f_2 alone. It clearly differs from the mean velocity field given in figure 2(*b*), when only f_1 is excited. The coordinate reference frame for these plots is given in Miksad (1972, figure 1*b*).

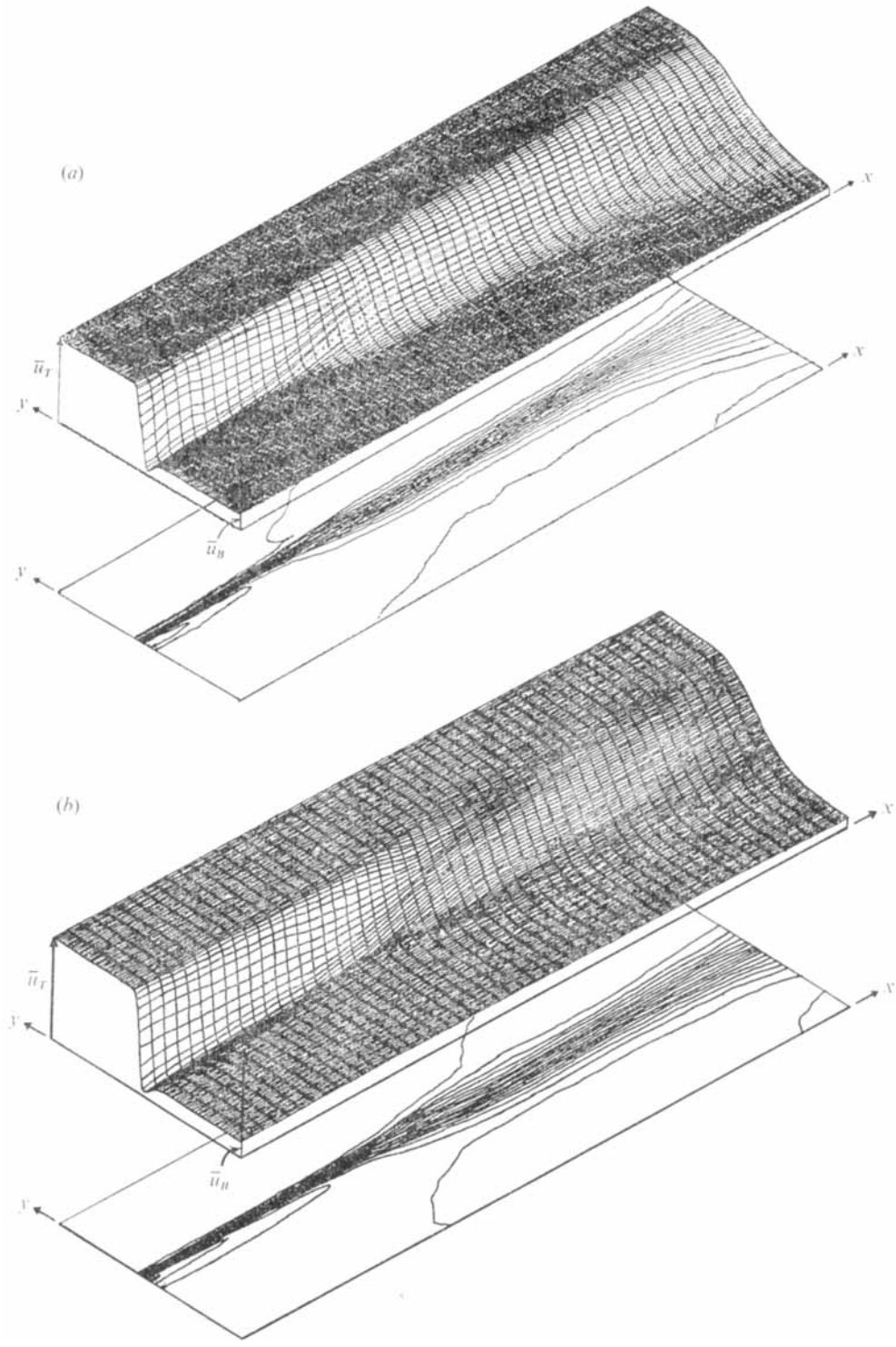

FIGURE 2. (*a*) Vertical profiles of mean velocity $\bar{u}(x, y)$ and contours of constant velocity when f_1 and f_2 are simultaneously excited. $f_1 = 22$ Hz, $f_2 = 29{\cdot}5$ Hz. Contour interval is $\bar{u}/\bar{u}_T = 0{\cdot}05$. $\bar{u}_T = 201$ cm/s, $\bar{u}_B = 38$ cm/s, $R_e = \Delta\bar{u}.\theta_b(x_0)/\nu = R(x_0) = 145$. (*b*) Vertical profiles and contours of $\bar{u}(x, y)$ when $f_1 = 22{\cdot}5$ Hz is excited. $R(x_0) = 145$.

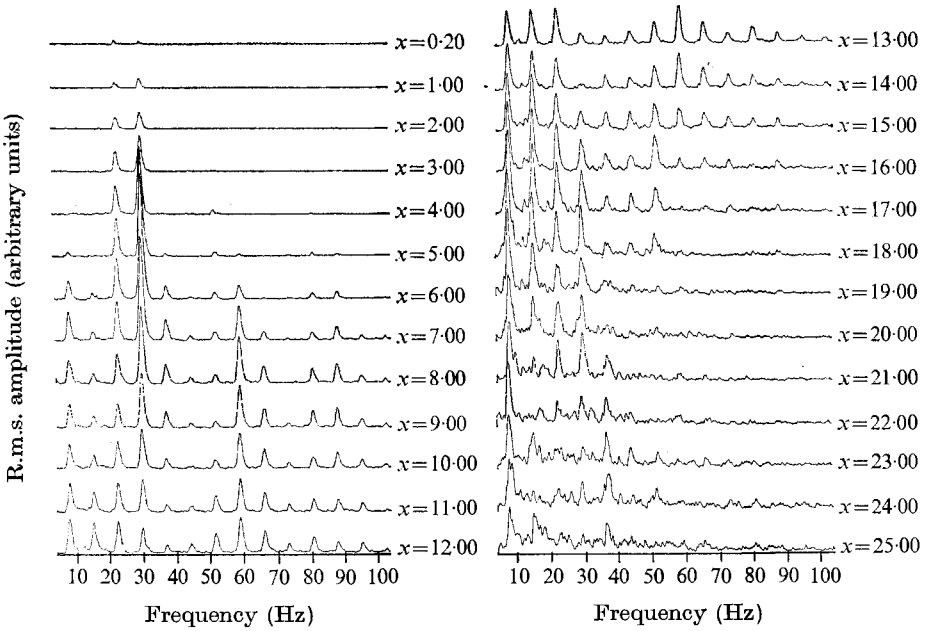

FIGURE 3. R.m.s. frequency spectra when f_1 and f_2 are simultaneously excited. y = 0·2 cm, f_1 = 22 Hz, f_2 = 29·5 Hz, $R(x_0)$ = 150, filter bandwidth = 1·0 Hz, sweep speed = 0·55 Hz/s, time constant = 1 s. x measured in centimetres.

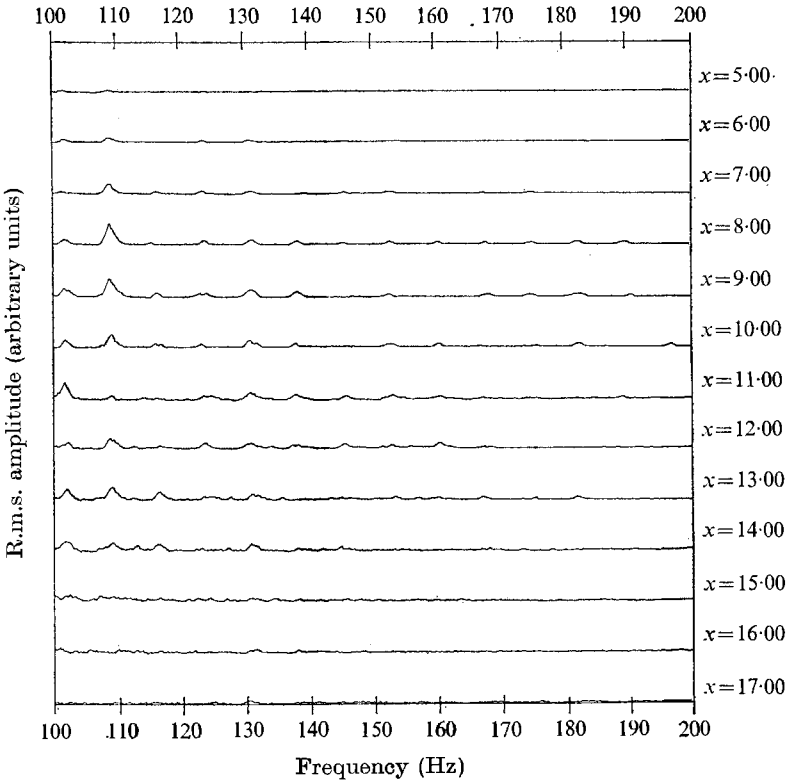

FIGURE 4. Spectra of higher frequency components when f_1 and f_2 are simultaneously excited. f_1 = 22 Hz, f_2 = 29·5 Hz, y = 0·2 cm, $R(x_0)$ = 150. x measured in centimetres.

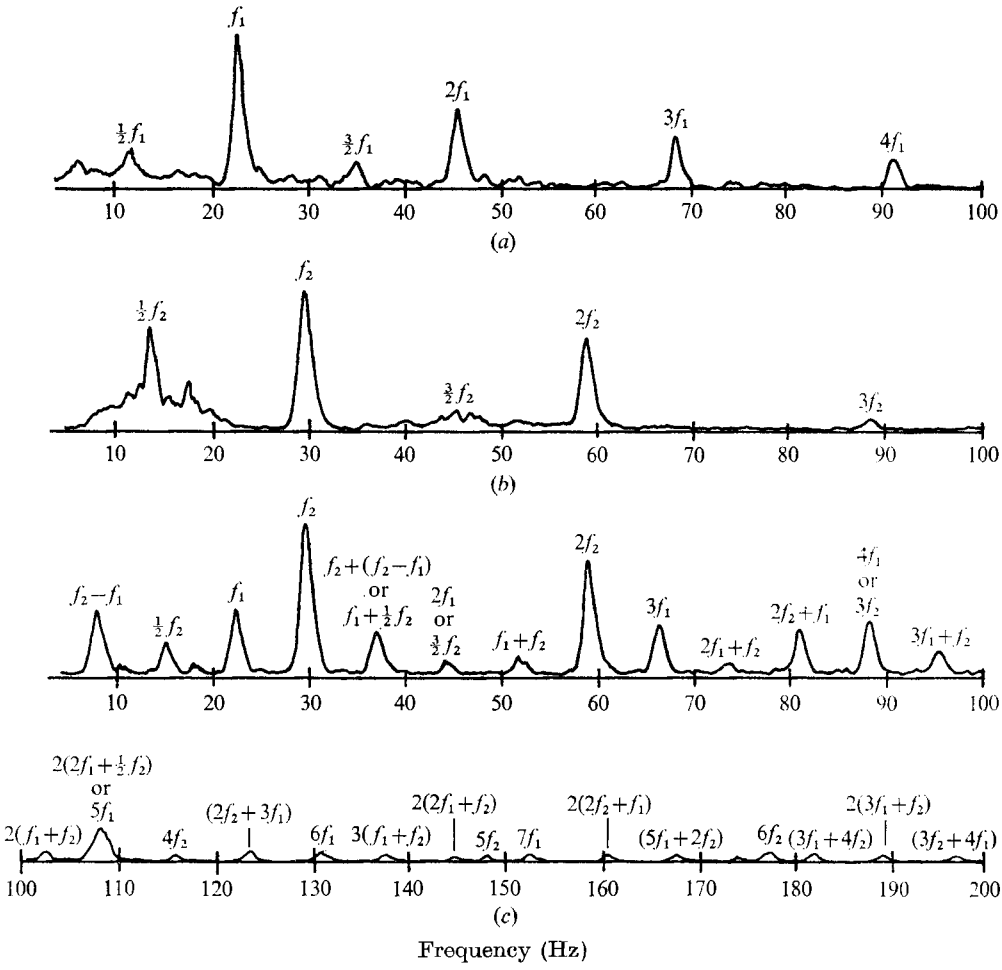

FIGURE 5. Representative frequency components in the instabilities resulting from excitation at (*a*) $f_1 = 22{\cdot}5$ Hz alone; (*b*) $f_2 = 29{\cdot}5$ Hz alone; (*c*) $f_1 = 22$ Hz and $f_2 = 29{\cdot}5$ Hz simultaneously. $R(x_0) = 150$.

4. Experimental results

Figure 3 shows frequency spectra of streamwise velocity fluctuations when f_1 and f_2 are excited at equal initial amplitudes. The two disturbances grow simultaneously. At $x = 4{\cdot}00$ cm small fluctuations at 52 Hz, the sum frequency f_2+f_1, are noticeable. Fluctuations near 7·5 Hz, the difference frequency f_2-f_1, appear at $x = 5{\cdot}00$ cm, and by $x = 7{\cdot}00$ cm fluctuations at other sum and difference frequencies $(nf_2/m) \pm (pf_1/q)$, $n, p = 1, 2, 3, \ldots$, $m, q = 1, 2$, are present in the spectra. Harmonics and subharmonics of f_1 and f_2 can also be identified. Figure 4 uses the same amplitude scale as figure 3, and shows the presence of many small amplitude fluctuations in the 100–200 Hz range. In all, more than 29 frequency components can be identified in the instability spectra.

Figure 5 shows three representative spectra taken during excitation at

Mode	Frequency (Hz)	Max $u'_{\text{r.m.s.}}/u_T$	Signal clarity
f_1	22	0·035	Very sharp
f_2	29·5	0·110	Very sharp
f_2-f_1	7·5	0·150	Sharp
$\frac{1}{2}f_1$	11	0·002	Barely detectable
$\frac{1}{2}f_2$	14·75	0·085	Somewhat intermittent
$f_1+\frac{1}{2}f_2$ or $f_2+(f_2-f_1)$	37	0·030	Sharp
$2f_1$ or $\frac{3}{2}f_2$	44	0·012	Somewhat intermittent
f_2+f_1	51·5	0·020	Sharp
$2f_2$ or $2f_1+\frac{1}{2}f_2$	59	0·046	Very sharp
$3f_1$	66	0·013	Sharp
$2f_1+f_2$	73·5	0·011	Somewhat intermittent
$2f_2+f_1$	81	0·012	Sharp
$3f_2$	88·5	0·013	Sharp
$3f_1+f_2$	95·5	0·010	Sharp
$2(f_2+f_1)$	103	0·008	Somewhat intermittent

TABLE 1. Maximum $u'_{\text{r.m.s.}}/\bar{u}_T$ amplitudes and signal clarity for frequency components in the spectra of the instability excited at $f_1 = 22$ Hz and $f_2 = 29{\cdot}5$ Hz simultaneously

a) $f_1 = 22{\cdot}5$ Hz alone; (*b*) $f_2 = 29{\cdot}5$ Hz alone; and (*c*) $f_1 = 22$ Hz and $f_2 = 29{\cdot}5$ Hz simultaneously. The significant frequency components are labelled with the probable interaction which generated them. An indication of maximum $u'_{\text{r.m.s.}}$ amplitude and general signal clarity (based on lack of intermittency and sharpness of spectral energy concentration) is given in table 1.

The development of the transition, once nonlinear effects become important, can be followed in figure 6. In this plot, variations in $u'_{\text{r.m.s.}}(x, y)/\bar{u}_T$ with downstream distance (x), and vertical location (y) are given for significant frequency components. The splitter plate which forms the vertical shear layer is located at the mid-point of the y axis and lies in the $u'_{\text{r.m.s.}}/\bar{u}_T$, x axis plane. The x axis covers the entire range from initial instability to the onset of turbulent breakdown.

A more quantitative description of the transition is given in figure 7, where downstream values of $u'_{\text{r.m.s.}}/\bar{u}_T$ maxima are plotted for most of the frequency components generated by nonlinear interactions.

5. Discussion of the results

Figures 8 and 9 show the growth of $u'_{\text{r.m.s.}}$ maxima when the flow is excited at f_1 and at f_2 respectively. These two figures provide a reference for the development of instability in the absence of disturbance interactions. It is clear from figure 7 that the dual-excitation instability is not a simple superposition of the two individually excited instabilities. The transition is clearly influenced by disturbance interactions.

However, the overall development of instability has basic similarities to the case when disturbance interactions are not important. In downstream order, the following features are observed in the dual-excitation transition: (i) a small amplitude region where disturbances grow exponentially and independently;

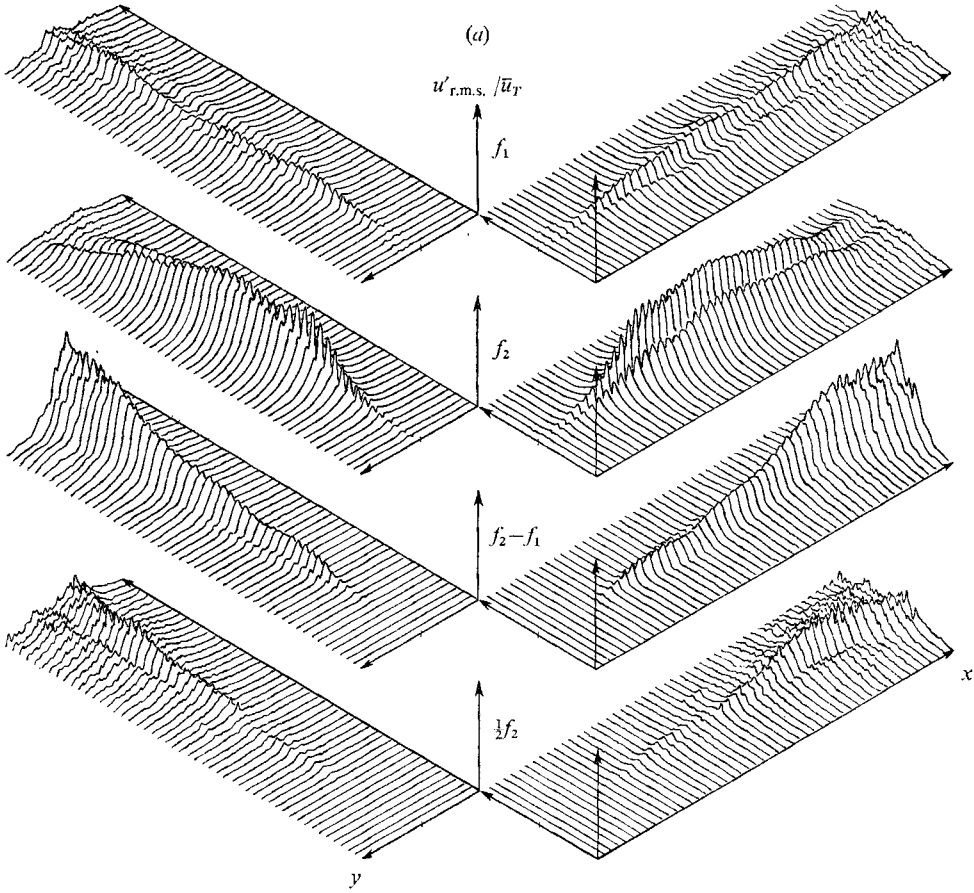

FIGURE 6(a). For legend see facing page.

(ii) a nonlinear region where harmonics, subharmonics and combination modes are generated and mode competition takes place; (iii) a region of finite amplitude equilibration of the growing disturbances; (iv) a second region of subharmonic and (f_2-f_1) difference-mode growth. Smoke trace and spanwise phase measurements then show that (v) three-dimensional distortions appear and develop into a streamwise vortex structure; (vi) secondary instabilities preceed the transition to turbulence.

A comparison of this brief description with that given by Miksad (1972) for instabilities excited at a single frequency will reveal the basic similarities. The major differences arise from disturbance interactions (i.e. combination-mode generation and mode competition) and the large number of frequency components which share the available fluctuation energy.

5.1. *Small amplitude growth and the breakdown of linear superposition*

Table 2 shows spatial growth rates $-\alpha_i$ measured for several frequency components. The respective growth rates of f_1 and f_2 during dual excitation are close

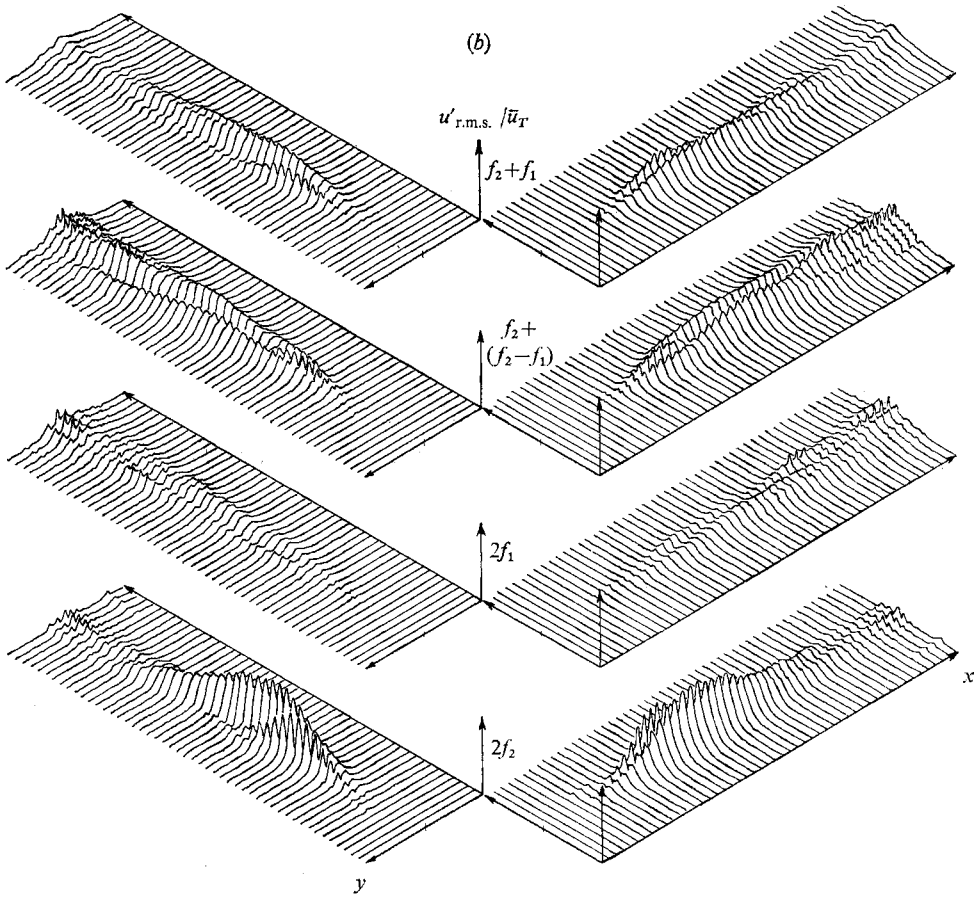

FIGURE 6. Vertical profiles of $u'_{\text{r.m.s.}}/\bar{u}_T$ for frequency components in the instability excited at $f_1 = 22$ Hz and $f_2 = 29{\cdot}5$ Hz simultaneously. $R(x_0) = 150$. Profiles made at 0·5 cm downstream intervals. (*a*) $f_1 = 22$ Hz, amplitude axis = 0·155 full scale; $f_2 = 29{\cdot}5$ Hz, 0·155 full scale; $f_2-f_1 = 7{\cdot}5$ Hz, 0·155 full scale; $\frac{1}{2}f_2 = 14{\cdot}75$ Hz, 0·155 full scale. (*b*) $(f_2+f_1) = 51{\cdot}5$ Hz, amplitude axis = 0·055 full scale; $f_2+(f_2-f_1) = 37$ Hz, 0·055 full scale; $2f_1 = 44$ Hz; 0·055 full scale; $2f_2 = 59$ Hz, 0·055 full scale.

to the values measured when each disturbance is individually excited. The growth rates of nonlinearly generated modes are measured from their point of generation.

Maximum $u'_{\text{r.m.s.}}/\bar{u}_T$ amplitudes of f_1 and f_2, shown in figure 7, are less than 0·02 during the first 3·00 cm. A comparison with figures 8 and 9 shows that, for $x < 3{\cdot}00$ cm, the dual-excitation instability is a superposition of the individually excited instabilities. The superposition breaks down as disturbances grow to large amplitudes and interact with each other. In the present experiments, the linear concept of superposition is only valid for disturbance amplitudes less than 0·02 times $\bar{u}_T$. This is a much smaller amplitude than that normally assumed for the breakdown of linear theory. It indicates a strong limitation on the applicability of linear approximations.

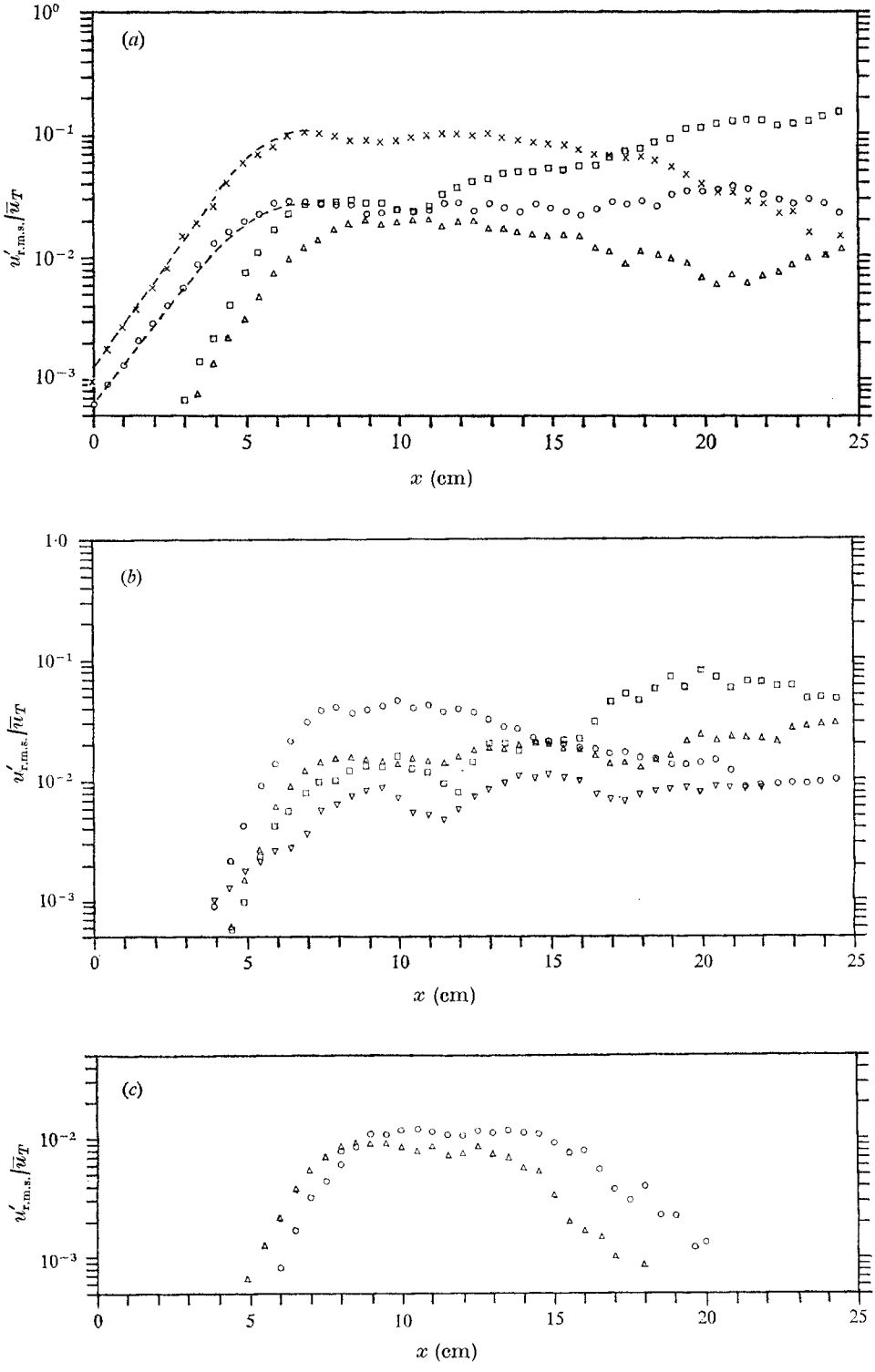

FIGURE 7(*a–c*). For legend see facing page

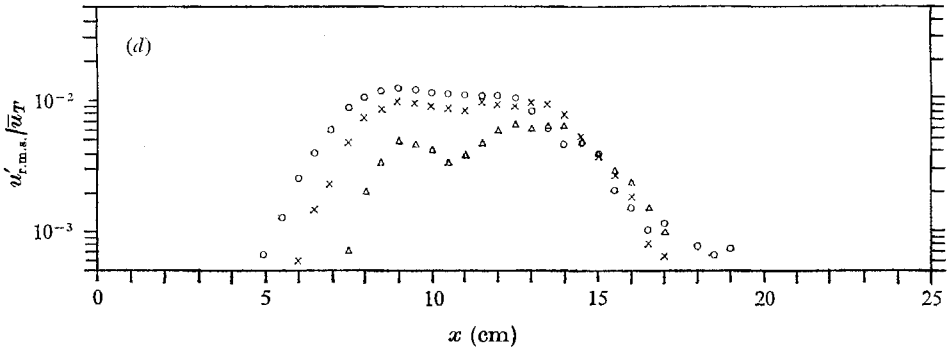

FIGURE 7. Downstream values of $u'_{\text{r.m.s.}}$ maxima in the instability excited at $f_1 = 22$ Hz and $f_2 = 29{\cdot}5$ Hz simultaneously. $R(x_0) = 150$. (*a*) ×, f_2; ○, f_1; □, $f_2 - f_1$; △, $f_2 + f_1$; – – –, numerical solutions of (5.1) and (5.2) when the experimentally determined Landau coefficients are used. (*b*) □, $\frac{1}{2}f_2$; △, $f_2 + (f_2 - f_1)$; ▽, $\frac{3}{2}f_2$; ○, $2f_2$. (*c*) ○, $3f_1$; △, $(2f_2 + f_1)$. (*d*) ○, $3f_2$; ×, $(2f_1 + f_2)$; △, $2(f_1 + f_2)$..

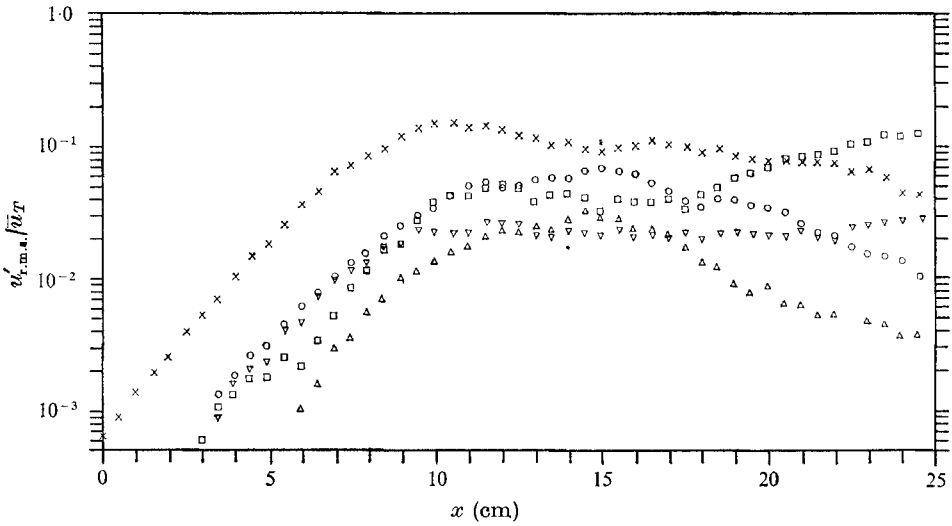

FIGURE 8. Downstream values of $u'_{\text{r.m.s.}}$ maxima in the instability excited at $f_1 = 22{\cdot}5$ Hz alone. ×, f_1; ○, $2f_1$; △, $3f_1$; □, $\frac{1}{2}f_1$; ▽, $\frac{3}{2}f_1$. $R(x_0) = 145$.

5.2. *Generation of combination modes*

The generation (or to be more accurate the first measurable appearance) of fluctuations at sum and difference frequencies $f_2 \pm f_1$ coincided with the emergence of second-harmonic fluctuations $2f_2$ and $2f_1$. Once the $2f_1$, $2f_2$ and $f_2 \pm f_1$ fluctuations had been generated, higher harmonics nf_1 and pf_2 ($n, p > 2$), subharmonic fluctuations $\frac{1}{2}f_1$ and $\frac{1}{2}f_2$ and additional combination modes of the form

$$(nf_2/m) \pm (pf_1/q) \quad (n, p = 1, 2, 3 \ldots;\ m, q \leqslant = 1, 2)$$

were generated in what appeared to be a continuous downstream sequence. The downstream intervals between new frequency components presumably represent the distance needed for previously generated fluctuations to grow to large enough

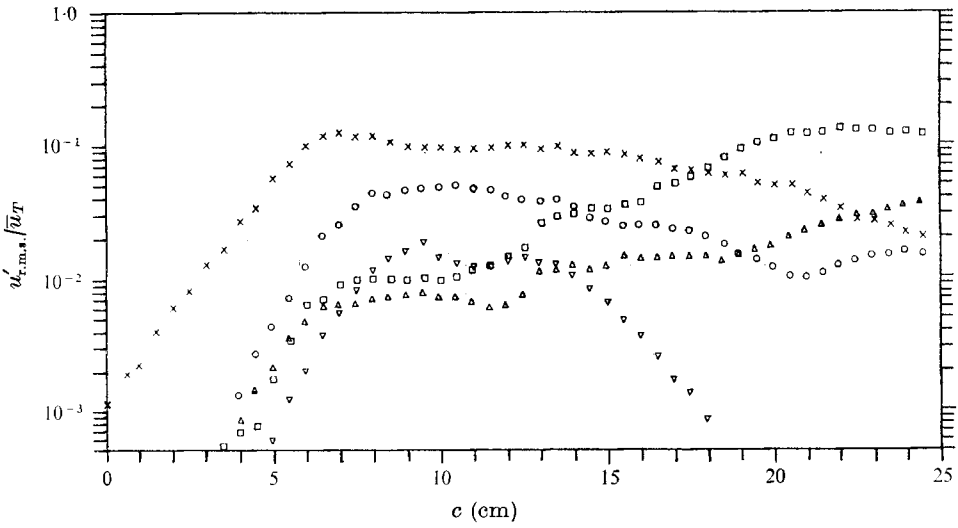

FIGURE 9. Downstream values of $u'_{\text{r.m.s.}}$ maxima in the instability excited at $f_2 = 29{\cdot}5$ Hz alone. $\times, f_2$; $\bigcirc, 2f_2$; $\bigtriangledown, 3f_2$; $\square, \frac{1}{2}f_2$; $\bigtriangleup, \frac{3}{2}f_2$. $R(x_0) = 145$. Data taken from Miksad (1972).

Mode	$-\alpha_i = -\alpha_i^* \times 2\theta_b(x_0)$	Mode	$-\alpha_i^* = -\alpha_i \times 2\theta_b(x_0)$
f_1	0·144	$\frac{1}{2}f_2$	0·285
f_2	0·198	$f_1+\frac{1}{2}f_2$ or $f_2+(f_2-f_1)$	0·276
f_2-f_1	0·246	$2f_1$ or $\frac{3}{2}f_2$	0·109
f_2+f_1	0·209	$2f_2$	0·220

TABLE 2. Initial exponential spatial growth rates $-\alpha_i$ of significant frequency components in the instability excited at $f_1 = 22$ Hz and $f_2 = 29{\cdot}5$ Hz simultaneously. Growth rate of f_1 measured when $f_1 = 22{\cdot}5$ Hz alone is excited is 0·138. Growth rate of f_2 when $f_2 = 29{\cdot}5$ Hz alone is excited is 0·200.

amplitudes for further interaction. For example, in figure 6, we can see that the frequency component due to the interaction of f_2 with the difference mode only appears after both f_2 and f_2-f_1 reach amplitudes sufficient for efficient interaction. Note also the nested pattern of growth and decay for successively higher frequency components (generated by higher order interactions) in figure 7.

It is also interesting to note in figure 7 that f_2-f_1 and $\frac{1}{2}f_2$ both enter a second region of growth at $x = 11{\cdot}00$ cm. This second region of growth occurs only after the two fundamentals equilibrate into relatively constant amplitude fluctuations. Kelly (1967) showed that this second region of $\frac{1}{2}f_2$ subharmonic growth may be due to the finite amplitude oscillations of f_2. His mechanism involved the interaction of two disturbances to give a subharmonic component. A similar mechanism may trigger the post-equilibration growth of f_2-f_1.

In identifying probable interactions in table 1, most combination-mode fluctuations are assumed to result from the interaction of f_1 and f_2 with each other, with each other's harmonics and subharmonics, and with previously generated combination modes. However, combination modes can also arise from interac-

tions which do not include f_1 and f_2 directly. The 59 Hz fluctuation, for example, could result from an interaction of $2f_1$ with $\frac{1}{2}f_2$.

The choice of $f_1 = 22$ Hz made it impossible to discriminate between $2f_1 = 44$ Hz and $\frac{3}{2}f_2 = 44{\cdot}25$ Hz. The behaviour of fluctuations at 44 Hz, however, indicate that $2f_1$ and $\frac{3}{2}f_2$ are both present. Each seems to dominate in the region of transition best suited to its dynamics. For example, the strong initial growth and sharp energy concentration of fluctuations at 44 Hz prior to equilibration, and their tendency to decay after equilibration, is similar to the behaviour of $2f_1$ when f_1 alone is excited. However, after a small period of post-equilibration decay (see figure 10), the 44 Hz fluctuation encounters a second region of strong growth, just as $\frac{3}{2}f_2$ does when f_2 alone is excited.

5.3. *Influence of disturbance interactions on finite amplitude equilibration*

In figure 7 the growth of f_1 can be seen to deviate from its initial exponential rate at $x = 4{\cdot}00$ cm. In contrast the growth rate of f_2 in figure 7 remains unchanged at $x = 4{\cdot}00$ cm. The amplitude of f_2 in figure 7 at $x = 4{\cdot}00$ cm is $u'_{\text{r.m.s.}}/\overline{u}_T = 0{\cdot}02$, more than twice that of f_1, and it is clearly the dominant disturbance. It is worth noting in figure 8 that the growth of f_1 is unchanged at $x = 4{\cdot}00$ cm when it is individually excited. The growth of f_1 during dual excitation is clearly influenced by the finite amplitude fluctuations of f_2.

At $x = 5{\cdot}00$ cm, the growth of f_2 also starts to deviate from its initial exponential rate, and f_2 joins f_1 in equilibrating into constant amplitude fluctuations at $x = 7{\cdot}00$ cm. The equilibration amplitude of f_2 is $u'_{\text{r.m.s.}}/\overline{u}_T = 0{\cdot}108$, which is slightly less than the value of $u'_{\text{r.m.s.}}/\overline{u}_T = 0{\cdot}12$ measured when f_2 alone is excited (see figure 9). The equilibration amplitude of f_1 is $u'_{\text{r.m.s.}}/\overline{u}_T = 0{\cdot}0237$, and is much smaller than the value of $u'_{\text{r.m.s.}}/\overline{u}_T = 0{\cdot}14$ measured when f_1 alone is excited (see figure 8 also).

In general, the growth and equilibration of f_2 (during dual excitation) is only slightly influenced by the small amplitude fluctuations of f_1. This can be seen by comparing figures 7 and 9.

The phenomena of growing disturbances equilibrating into constant finite amplitude oscillations is observed in many fluid flows. Taylor (1923) and Coles (1965), amongst others, have observed that growing perturbations in the flow between two rotating cylinders eventually equilibrate into constant amplitude oscillations (the so-called Taylor vortices). Similar steady finite amplitude motions are also observed in the form of Bénard cells in thermal convective instability.

Stuart (1962) showed that the basic features of the dual-mode equilibration process can be identified in a simple model which considers the interaction of two disturbances f_1 and f_2 in a parallel flow. The equations governing the two disturbances can be shown (see Stuart 1962) to have the form of two coupled Landau equations:

$$d|A|^2/dx = 2|A|^2\{-\alpha^*_{iA} + a^*_A|A|^2 + a^*_B|B|^2\}, \tag{5.1}$$

$$d|B|^2/dx = 2|B|^2\{-\alpha^*_{iB} + b^*_B|B|^2 + b^*_A|A|^2\}. \tag{5.2}$$

A and B are the amplitudes of f_1 and f_2, and $-\alpha_{iA}^*$ and $-\alpha_{iB}^*$ are their initial exponential spatial growth rates. The self-Landau coefficients a_A^* and b_B^* represent nonlinear mechanisms which limit disturbance growth, whether or not a second disturbance is present. The cross-Landau coefficients a_B^* and b_A^* represent the additional constraints imposed by disturbance interactions. The equilibration of f_1 and equilibration of f_2 are linked through their nonlinear interaction. Mode competition, combination-mode generation, mean flow distortion and harmonic-mode generation influence the equilibration process.†

At equilibration, $d|A|^2/dx = 0$, $d|B|^2/dx = 0$ and equations (5.1) and (5.2) have the four solutions (see Stuart 1962)

$$|A_e|^2 = 0, \quad |B_e|^2 = 0; \tag{5.3}$$

$$|A_e|^2 = \alpha_{iA}^*/a_A^*, \quad |B_e|^2 = 0; \tag{5.4}$$

$$|A_e|^2 = 0, \quad |B_e|^2 = \alpha_{iB}^*/b_B^*; \tag{5.5}$$

$$|A_e|^2 = \frac{\alpha_{iA}^* b_B^* - \alpha_{iB}^* a_B^*}{b_B^* a_A^* - b_A^* a_B^*}, \quad |B_e|^2 = \frac{\alpha_{iB}^* a_A^* - \alpha_{iA}^* b_A^*}{b_B^* a_A^* - b_A^* a_B^*}. \tag{5.6}$$

Solution (5.3) implies that f_1 and f_2 are not unstable modes or are not excited. Solutions (5.4) and (5.5) represent the single-excitation experiments when f_1 and f_2 are individually excited. Solution (5.6) represents the dual-excitation experiments.

The self-Landau coefficients a_A^* and b_B^* can be determined from the initial growth rates and equilibration amplitudes of the single-excitation experiments. In dimensionless form

$$a_A = -5{\cdot}75, \quad b_B = -12{\cdot}8.$$

Using these values for a_A and b_B and the growth rates and equilibration amplitudes measured in the dual-excitation experiments, equations (5.1) and (5.2) can be solved at equilibration for a_B and b_A. In dimensionless form

$$a_B = -12{\cdot}15, \quad b_A = -90.$$

The calculated values of self- and cross-Landau coefficients represent amplitude-dependent mechanisms and only have meaning when weighted with the appropriate disturbance amplitudes. The amplitude-weighted terms in the coupled Landau equations have the following values at equilibration.

$$\text{Theory:} \qquad -\alpha_{iA} + a_A|A_e|^2/\bar{u}_T^2 + a_B|B_e|^2/\bar{u}_T^2 = 0.$$

$$\text{Experiment:} \qquad [0{\cdot}144] - [0{\cdot}0031] - [0{\cdot}141] \simeq 0.$$

† Finite amplitude mode competition and reduced equilibration amplitudes also occur in thermal plasma instability. Lashinsky (1965) showed that the energies of two growing modes in a thermal plasma are governed by equations similar to (5.1) and (5.2). His experiments also show that the eventual equilibration amplitudes of the two modes are determined by the extent of their interaction with one another, and by their initial exponential growth rates. In plasma instability, $-\alpha_{iA}$ and $-\alpha_{iB}$ again represent initial linear theory growth rates; a_A and b_B represent inherently nonlinear self-damping plasma mechanisms such as ion Landau damping; and a_B and b_A represent mode-coupling damping effects.

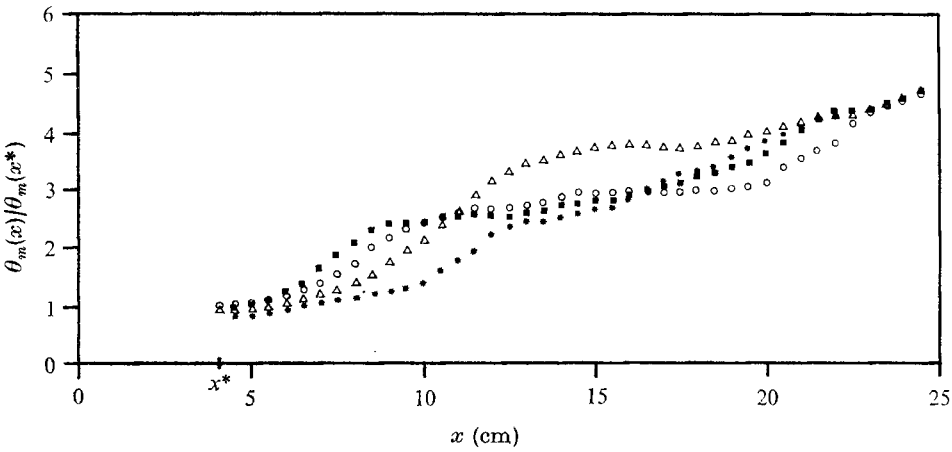

FIGURE 10. Downstream values of shear-layer momentum thickness after wake deficit is eliminated. *, natural instability; △, instability excited at $f_1 = 22{\cdot}5$ Hz alone; ○, instability excited at $f_2 = 29{\cdot}5$ Hz alone; ■, instability excited at $f_1 = 22$ Hz and $f_2 = 29{\cdot}5$ Hz simultaneously.

$$\text{Theory:} \qquad -\alpha_{iB} + b_B|B_e|^2/\bar{u}_T^2 + b_A|A_e|^2/\bar{u}_T^2 = 0.$$

$$\text{Experiment:} \qquad [0{\cdot}198] - [0{\cdot}148] - [0{\cdot}5] \doteq 0.$$

The model we have used to compute the Landau coefficients is for a parallel flow. Ru-Sue Ko, Kubuta & Lees (1970) considered the influence of mean flow spreading on the equilibration process in wakes. It is not clear from our results whether the influence of spreading in free-shear-layer equilibration is small or is counterbalanced by other dynamic processes.

It should be noted that the unweighted self- and cross-Landau coefficients represent potential growth limiting mechanisms. The potential realized depends on disturbance amplitude. Thus, although b_A is potentially larger that a_B we see from the weighted terms that the actual influence of f_2 on the equilibration of f_1 is twice as great as that of f_1 on the equilibration of f_2.

Additional less systematic and quantitative experiments (in which the relative initial amplitudes of f_1 and f_2 were varied) indicated that A_e and B_e are sensitive to changes in initial conditions. For example, in the experiments just described, the excitation amplitudes of f_1 and f_2 were set equal to each other and to the value used in the single-excitation experiments. The larger growth rate of f_2 ensured that it reached a finite amplitude first, and the equilibration amplitude of f_1, the smaller amplitude fundamental, was reduced. If, however, f_1 was excited at a large amplitude relative to f_2 it grew to finite amplitude first and the equilibration amplitude of f_2 was reduced. If the excitation amplitudes were adjusted so that both disturbances reached finite amplitude together, the equilibration amplitudes of both components tended to be reduced, but not as strongly as when one component is clearly dominant. This latter behaviour has also been observed by Sato (1970) in symmetric wakes. In general, mode competition and growth suppression seems to be determined by the disturbance which reaches finite amplitudes of order $u'_{\text{r.m.s.}}/\bar{u}_T = 0{\cdot}02$ to $0{\cdot}03$ first.

The importance of initial conditions (or external conditions as in experiments in which artificial excitation is used) on wavenumber selection has also been observed in centrifugal and thermally driven instabilities. Snyder (1969) notes that the wavenumber of finite amplitude secondary motion in the Taylor-vortex problem is sensitive to initial conditions. This can also be seen in the experiments of Coles (1965). Chen & Whitehead (1968) found that thermal convective motions corresponding to wavenumbers other than the value at critical Rayleigh number can be obtained by selective external forcing before the critical Rayleigh number is reached. Similar results have been obtained on theoretical grounds by Newell & Whitehead (1969) and Newell, Lange & Aucoin (1970).

5.4. *Influence of mean flow distortions*

Mean flow distortions can play an important role in finite amplitude equilibration (see Stuart 1958). Figure 10 shows downstream changes in the shear-layer momentum thickness. Note the similarity of the development of the shear layer during dual excitation and during excitation at f_2 only. The abrupt increase in θ_m at $x = 5{\cdot}00$ cm coincides with deviation from exponential growth and the onset of equilibration.

The amplitudes of f_1 and of f_2 (when both are excited) are of order $u'_{\text{r.m.s.}}/\bar{u}_T = 0{\cdot}02$ and 0·06 respectively at the onset of spreading. It is interesting to note that the amplitude of f_2 (when it alone is excited) is also of order $u'_{\text{r.m.s.}}/\bar{u}_T = 0{\cdot}06$ at the onset of spreading. The dominance of f_2 in both experiments and the basic similarity in mean flow development suggest that spreading in both cases is determined by the finite amplitude Reynolds stress of f_2. The slightly faster rate of spreading measured during dual excitation seems to be mainly due to the additional distortions caused by the small amplitude fluctuations of f_1.

The experiments of Miksad (1972) also point to the importance of mean flow distortions in the equilibration process during single-mode excitation. The similarity of the shear-layer development during dual excitation and during f_2 excitation suggests that the major influence of f_2 on the growth and equilibration of f_1 may be due to the dominant distortion of the mean flow by f_2. This leads to a velocity field which is apparently unsuitable for f_1 growth. The additional presence of small amplitude fluctuations of f_1 only serve to distort the mean flow even more from the pattern observed during f_1 excitation. Presumably, the mean flow development during f_1 excitation is most efficient for f_1 growth and it is not surprising that, in a velocity field similar to that observed when f_2 is excited, the growth and equilibration of f_2 is not significantly changed, while that of f_1 is drastically altered.

5.5. *Spectral distribution of fluctuation energy*

The vertically integrated $u'^2_{\text{r.m.s.}}/\bar{u}^2_T$ energy of various frequency components in the dual excitation and the single-mode excitation instabilities are plotted in figures 11, 12 and 13; where for a given frequency component

$$E_u(x) = \int_{-L}^{L} \frac{u'^2_{\text{r.m.s.}}(x, y)}{2\bar{u}^2_T \cdot \theta_b(x_0)}\, dy,$$

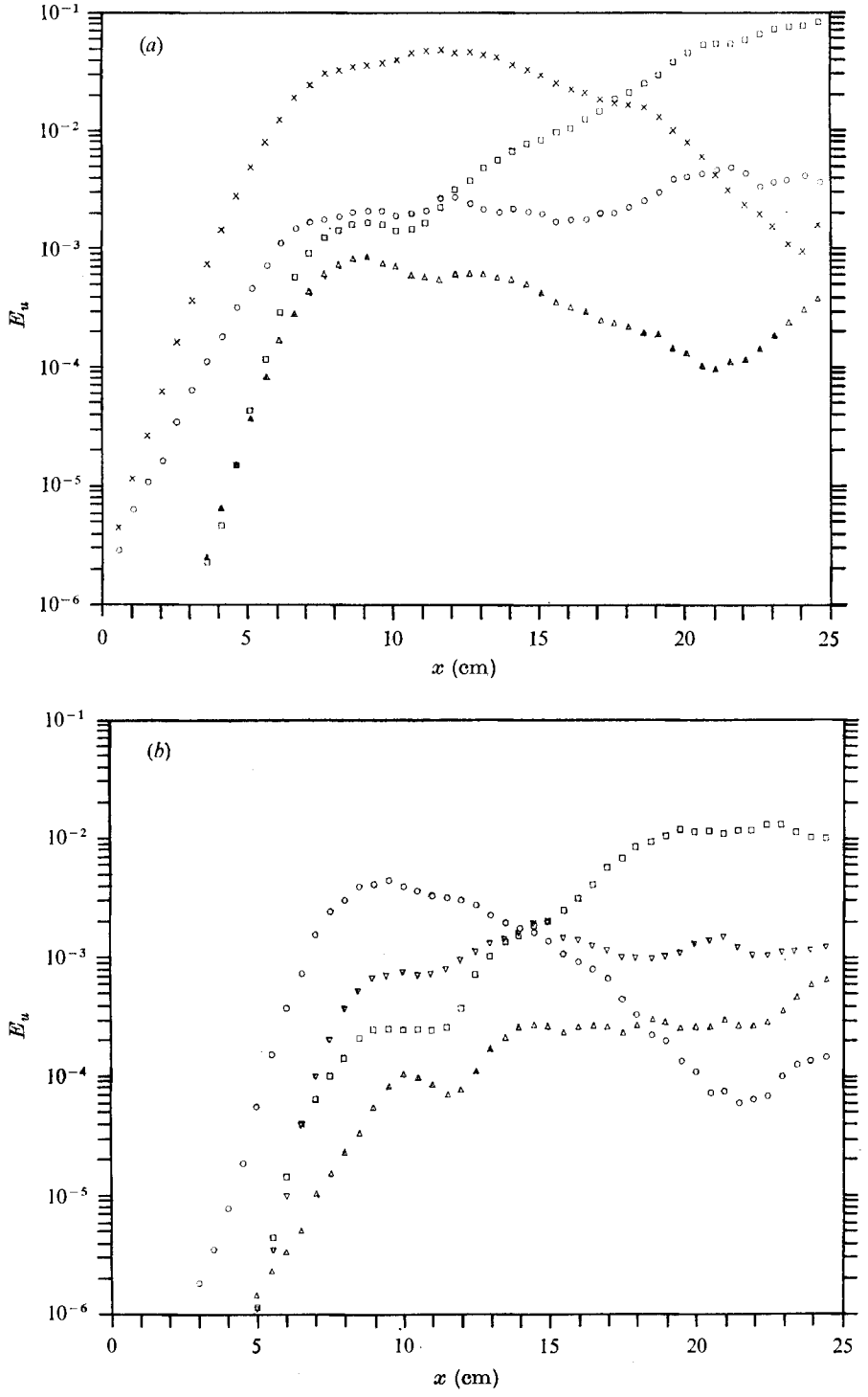

FIGURE 11. Downstream values of E_u for various frequency components in the instability excited at $f_1 = 22$ Hz and $f_2 = 29{\cdot}5$ Hz simultaneously. (*a*) ○, f_1; ×, f_2; □, f_2-f_1; △, f_2+f_1. $R(x_0) = 150$. (*b*) □, $\frac{1}{2}f_2$; ▽, $f_2+(f_2-f_1)$; △, $2f_1$ or $\frac{3}{2}f_2$; ○, $2f_2$. $R(x_0) = 150$.

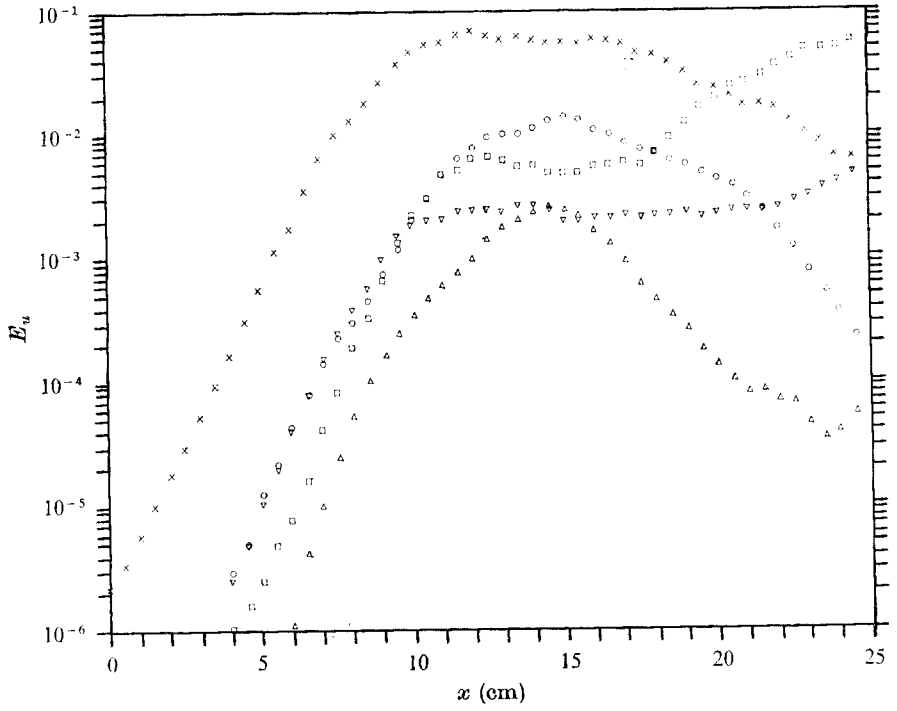

FIGURE 12. Downstream values of E_u for various frequency components in the instability excited at $f_1 = 22{\cdot}5$ Hz alone. $\times$, f_1; $\bigcirc$, $2f_1$; $\triangle$, $3f_1$; $\square$, $\frac{1}{2}f_1$; ∇, $\frac{3}{2}f_1$. $R(x_0) = 145$.

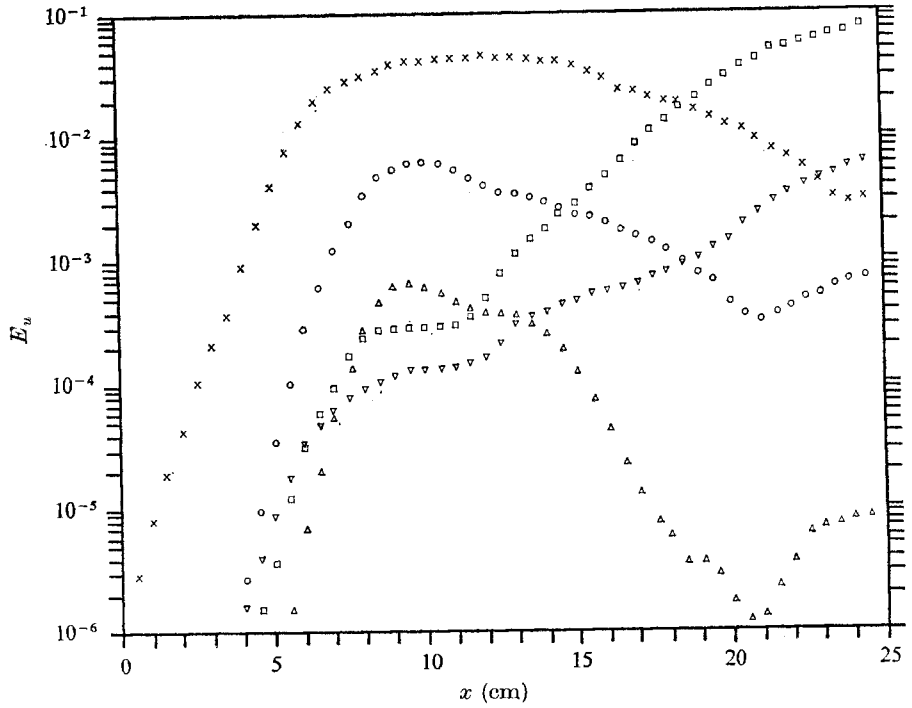

FIGURE 13. Downstream values of E_u for various frequency components in the instability excited at $f_2 = 29{\cdot}5$ Hz alone. $\times$, f_2; $\bigcirc$, $2f_2$; $\triangle$, $3f_2$; $\square$, $\frac{1}{2}f_2$; ∇, $\frac{3}{2}f_2$. $R(x_0) = 145$. Data taken from Miksad (1972).

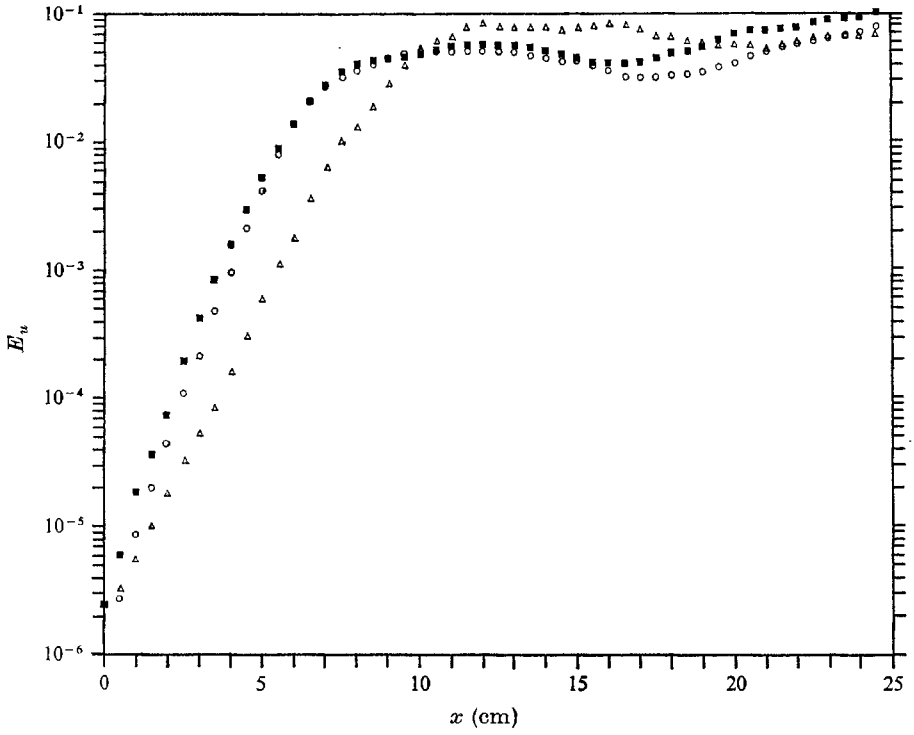

FIGURE 14. Downstream values of total disturbance energy E_u^T, defined as the sum of the respective E_u energies of all frequency components present in each instability. △, instability excited at $f_1 = 22{\cdot}5$ Hz alone; ○, instability excited at $f_2 = 29{\cdot}5$ Hz alone; ■, instability excited at $f_1 = 22$ Hz and $f_2 = 29{\cdot}5$ Hz simultaneously.

L is much larger than the shear-layer thickness, and $\theta_b(x_0)$ is the sum of the momentum thicknesses of the two boundary layers prior to merging at the splitter plate edge.

In comparing the development of the spectral distribution of $u'_{\text{r.m.s.}}$ energy in the dual-excitation instability (see figure 11) with that of the two single-excitation instabilities in figures 12 and 13, one notices a lack of consistency in the allocation of energy amongst the various components. Many additional frequency components are present in the dual instability, and although the harmonics and subharmonics of f_2, the dominant fundamental, tend to dominate, no obvious overall allocation pattern can be identified. The maximum energy of $2f_1$ in the dual instability, for example, is almost two orders of magnitude smaller than that of $2f_1$ in the f_1 single-excitation instability. Also, although $\frac{1}{2}f_2$ tends to have the same initial pattern of development in the dual-excitation and f_2 single-excitation instabilities, it is the difference mode $f_2 - f_1$ which dominates the downstream stages of the dual instability.

In considering the meaning of these differences in spectral energy development, we must bear in mind that all three instabilities are heading towards the same end state – namely turbulence – which we do not expect to depend on initial conditions or the manner of instability which leads to it. This in fact seems

to be true in the present experiments, as spectra taken far downstream, where the flow has become turbulent, show the same basic distribution of energy in each instability.

There is another feature of the flow, however, which, even before turbulence is reached, does not seem to depend on initial conditions, or the details of instability. Namely, the total energy E_u^T of all $u'_{\text{r.m.s.}}$ fluctuations once nonlinear effects dominate the flow, where E_u^T is defined as the sum of the integrated E_u energy of all major frequency components in the disturbance spectra.

Measurements of total fluctuation energy E_u^T are shown in figure 14. They indicate that in each instability the sum of the energies of all frequency components has an upper bound of roughly $E_u^T = 0{\cdot}1$. It is significant to note that the total energy available to fluctuations does not depend on the number of disturbances that are excited, or subsequently generated by nonlinear interactions. This is particularly striking when one considers that the number of nonlinear modes and the allocation of energy per frequency component in the dual-excitation instability is quite different from that of the f_1 or f_2 instabilities. Each instability distributes its available energy among all generated fluctuations. The absence of a consistent energy allocation pattern indicates that the important constraint on fluctuation energy is the total energy available, and this in turn must be determined by the mean flow. An increase in the number of frequency components does not lead to an increase in fluctuation energy. Instead, a redistribution of available energy takes place.

6. Conclusions

The experiments show that significant interactions take place between disturbances in a laminar free shear layer. The instability when two disturbances are excited differs in detail from that measured when only one disturbance is excited. However, the overall development of instability remains the same and seems to be dictated by the mean flow. The interaction of disturbances leads to the generation of numerous combination modes of the form $(nf_2/m) \pm (pf_1/q)$, $n, p = 1, 2, 3, \ldots$, $m, q = 1, 2$, and to nonlinear-mode competition. The latter behaviour depends on the relative amplitudes of the interacting disturbances, and in general the dominant disturbance tends to suppress the growth of the other. Disturbance interactions influence the process of finite amplitude equilibration and the results suggest that mean flow distortions may play a primary role in the equilibration process. Evidence of finite amplitude triggered instability of the difference mode $f_2 - f_1$ is found, and the mechanism may be similar to that described by Kelly (1967) for the subharmonic mode. The total energy available to disturbance fluctuations has an upper bound which does not seem to depend on the number of disturbances excited or subsequently generated by nonlinear interactions. If many frequency components are generated, as in the dual-excitation instability, the disturbance energy is redistributed and not increased.

The sensitivity of wavenumber selection (in the nonlinear stages of instability) to initial and external conditions noticed in this experiment, as well as by Sato (1970) and in the experiments of Snyder (1969) and Coles (1965) on centrifugal

instabilities and Chen & Whitehead (1968) on thermal instabilities, points out one shortcoming of externally excited instability experiments. Namely, although external excitation allows one to conduct experiments which model certain explicit features of theoretical models, one is faced with the problem of recognizing that in weighting the initial disturbance field in favour of a particular wavenumber (or pair of wavenumbers) one may force the instability into a configuration that natural selection processes may not necessarily choose. The resulting experimental data must only be interpreted in terms of the constraints one has imposed on the flow. The importance of imposed experimental constraints cannot be over emphasized. One simple example is the great difference in the shear-layer instabilities excited at one frequency and at two frequencies simultaneously. In the latter case an additional constraint is imposed when one chooses the relative phase between the two excitation frequencies. Other experiments, not reported in this paper, showed that the details of dual-excitation instability, such as the strength and order of combination-mode generation, vary as the relative phases of the two excitation signals are changed.

The author would like to thank the National Science Foundation and the Science Research Council of England for their support of this research. The valuable suggestions of Professor J. T. Stuart and other members of the Department of Mathematics, Imperial College, are deeply appreciated.

REFERENCES

CHEN, M. & WHITEHEAD, J. 1968 *J. Fluid Mech.* **31**, 1.
COLES, D. 1965 *J. Fluid Mech.* **21**, 315.
KELLY, R. E. 1967 *J. Fluid Mech.* **27**, 657.
LASHINSKY, H. 1965 *Phys. Rev. Lett.* **14**, 1064.
MIKSAD, R. W. 1972 *J. Fluid Mech.* **56**, 695.
NEWELL, A. C., LANGE, C. G. & AUCOIN, P. J. 1970 *J. Fluid Mech.* **40**, 513.
NEWELL, A. C. & WHITEHEAD, J. 1969 *J. Fluid Mech.* **38**, 279.
RU-SUE KO, D., KUBUTA, T. & LEES, L. 1970 *J. Fluid Mech.* **40**, 315.
SATO, H. 1970 *J. Fluid Mech.* **44**, 741.
SNYDER, H. 1969 *J. Fluid Mech.* **35**, 273.
STUART, J. T. 1958 *J. Fluid Mech.* **4**, 1.
STUART, J. T. 1962 *Proc. Int. Congr. Appl. Mech., Stresa*, pp. 63–97. Elsevier.
TAYLOR, G. I. 1923 *Phil. Trans.* A **223**, 289.